Geophysical Research Letters

RESEARCH LETTER
10.1029/2023GL105517

Time-Dependent Weakening of Granite at Hydrothermal Conditions

T. N. Jeppson[1], D. A. Lockner[1], N. M. Beeler[1], and D. E. Moore[1]

[1]U.S. Geological Survey, Earthquake Science Center, Menlo Park, CA, USA

Key Points:

- Time-dependent weakening of simulated fault surfaces at hydrothermal conditions is observed
- Weakening mechanism is water-assisted, temperature-dependent, and depends on host rock composition
- Capturing frictional behavior across all time scales requires a rate and state model with two state variables and a time delay parameter

Supporting Information:

Supporting Information may be found in the online version of this article.

Correspondence to:

T. N. Jeppson,
tjeppson@usgs.gov

Citation:

Jeppson, T. N., Lockner, D. A., Beeler, N. M., & Moore, D. E. (2023). Time-dependent weakening of granite at hydrothermal conditions. *Geophysical Research Letters*, *50*, e2023GL105517. https://doi.org/10.1029/2023GL105517

Received 25 JUL 2023
Accepted 26 OCT 2023

Author Contributions:

Conceptualization: T. N. Jeppson, D. A. Lockner
Data curation: T. N. Jeppson
Formal analysis: T. N. Jeppson, N. M. Beeler
Funding acquisition: T. N. Jeppson, D. A. Lockner
Investigation: T. N. Jeppson, D. A. Lockner, N. M. Beeler, D. E. Moore
Methodology: T. N. Jeppson, D. A. Lockner
Project Administration: D. A. Lockner
Supervision: D. A. Lockner
Writing – original draft: T. N. Jeppson

Abstract The evolution of a fault's frictional strength during the interseismic period is a critical component of the earthquake cycle, yet there have been relatively few studies that examine the time-dependent evolution of strength at conditions representative of seismogenic depths. Using a simulated fault in Westerly granite, we examined how frictional strength evolves under hydrothermal conditions up to 250°C during slide-hold-slide experiments. At temperatures ≤100°C, frictional strength generally increases with hold duration but, at 200 and 250°C, an initial increase in strength transitions to rapid time-dependent weakening for holds longer than 14 hr. Forward modeling of long hold periods at 250°C using the rate and state friction constitutive equations requires a second, strongly negative, state variable with a long evolution distance. This implies that significant hydrothermal alteration is occurring at 250°C, consistent with microstructural observations of dissolution and secondary mineral precipitation.

Plain Language Summary A fault can regain strength following an earthquake. The rates, conditions, and mechanisms by which this recovery of strength occurs are not well understood but they are critical to understanding earthquake recurrence and induced seismicity. By conducting a series of experiments in which a simulated fault alternates between shear displacement and quasi-stationary hold periods, we examine how fault strength evolves with time at temperatures up to 250°C. At elevated temperatures the fault initially strengthens but then weakens over long timescales. This weakening appears to be due to hydrothermal alteration, potentially including the precipitation of secondary minerals in the fault. Relating this observed weakening behavior and associated mechanisms to constitutive equations will facilitate modeling earthquake behavior in different materials and at variety of environmental conditions.

1. Introduction

Earthquakes are known to reoccur on the same fault at semi-regular intervals (Bakun & Lindh, 1985; Uchida & Bürgmann, 2019). When an earthquake occurs, the fault weakens, followed by a protracted period of strength recovery (i.e., healing) before another large earthquake can occur. Identifying the mechanisms and associated conditions that contribute to fault healing is a crucial part of understanding earthquake recurrence and has implications for both natural earthquakes and induced seismicity.

While it is widely accepted that hydrothermal reactions can change the strength and behavior of fault zones, studies examining the time-dependence of frictional strength in faults have been conducted predominantly at room temperature and often under nominally dry conditions (e.g., Carpenter et al., 2016; Dieterich, 1972; Tesei et al., 2012). Experiments examining at hydrothermal conditions have primarily focused on monomineralic quartz systems (Jeppson, Lockner, Beeler, & Hickman, 2023; Karner et al., 1997; Nakatani & Scholz, 2004; Tenthorey et al., 2003). In these studies on quartz, frictional strength increases with contact time. However, when mixtures of quartz and labradorite were examined, no time-dependent strengthening was observed (Olsen et al., 1998). Additionally, experiments examining the slip-rate dependence of frictional strength in Westerly granite at hydrothermal conditions revealed a complex relation among frictional strength, temperature, and slip rate (Blanpied et al., 1995, 1998). In polymineralic systems, greater chemical complexity may facilitate reactions that can impact the evolution of strength in complicated ways (e.g., Hickman & Evans, 1995; Meyer et al., 2006).

This study seeks to elucidate the process of strength evolution in a polymineralic natural fault system at hydrothermal conditions by conducting slide-hold-slide (SHS) experiments on samples of Westerly granite at intermediate temperatures associated with the upper seismogenic zone and the transition from aseismic to seismic slip. Contrary to expected behavior, we find that fault surfaces weaken during extended holds at temperatures

Writing – review & editing: T. N. Jeppson, D. A. Lockner, N. M. Beeler, D. E. Moore

≥200°C. This weakening appears to be the result of a solution-transfer mechanism that is temperature dependent and chemically complex.

2. Methods

Laboratory SHS tests consist of alternating periods of induced fault slip and quasi-static holds during which time-dependent strength recovery occurs. We express strength changes in terms of secant friction, $\mu = \tau/(\sigma_n - P_p)$, where τ and σ_n are shear and normal stress resolved on the fault surface and P_p is pore pressure. The magnitude of restrengthening ($\Delta\mu$) is quantified as the difference between the peak failure strength upon resumption of slip and the steady-state sliding strength preceding the hold. Triaxial SHS experiments were conducted at temperatures from 22 to 250°C (Table S1 in Supporting Information S1) on cylindrical (2.54 cm diameter) Westerly granite samples containing saw-cuts inclined at 30°. Simulated fault surfaces were roughened with #240 grit sandpaper to attain similar starting surfaces with RMS roughness of 5–10 μm. Tests were run at constant confining and pore pressures of 30 and 10 MPa, respectively. Deionized water was used as pore fluid and a 2.4 mm diameter borehole provided fluid access to the fault surface. A 24-hr thermal equilibration period preceded each experiment to allow the pore fluid and rock to approach chemical equilibrium.

The experiments began with 1 mm slip during whichh a thin (~5 μm) layer of ultrafine gouge developed. Multiple hold periods were then employed, separated by 250 μm of axial displacement at 0.1 μm/s. Hold durations ranged from 100 to 5×10^5 s and experiments were designed to repeat each hold duration up to three times. Mechanical data were corrected for elastic deformation of the loading system, jacket strength, the confining-pressure-dependence of piston seal friction, and the reduction in contact area during deformation as explained in Tembe et al. (2010). Further details of our experimental methodology can be found in Supporting Information S1 (Text S1).

3. Results

3.1. Friction Data

Sliding was stable at 22, 100, and 250°C (Figure 1; Figure S1 in Supporting Information S1) but oscillatory at 200°C where failure upon reloading was often associated with large stress drops (Figure 1c), consistent with previous studies on the frictional properties of Westerly granite at hydrothermal conditions (Blanpied et al., 1991, 1995). Due to the tendency for unstable slip, steady-state sliding friction at 200°C had to be extrapolated (Text S2 in Supporting Information S1). When stable sliding was observed it generally followed a consistent strain hardening trend (Figure 1; Figures S1 and S2 in Supporting Information S1). However, there are some exceptions. At 250°C, following holds ≥5,000 s, the sliding friction was initially less than the frictional strength preceding the hold period and the magnitude of the decrease in sliding friction increased with hold duration (Figure 1). The magnitude of strain hardening following hold periods longer than 50,000 s was noticeably greater than strain hardening following shorter holds (Figure S2 in Supporting Information S1) so that friction would presumably return to the pre-hold value, but this often required more than the alotted 250 μm of slip. Reductions in post-hold sliding friction, exceeding expected variation, were also seen at 100 and 200°C after 500,000 s holds (Figures 1f and 1g).

At temperatures from 22 to 200°C failure strength increased initially in proportion to the logarithm of hold duration (Figure 2), as reported in many previous studies for a variety of materials (e.g., Carpenter et al., 2016; Dieterich, 1972; Mitchell et al., 2013). Failure strength did not vary systematically with displacement (Figure S3 in Supporting Information S1). However, at 200°C for holds longer than 50,000 s the failure strength decreased with hold duration (Figure 2). This weakening behavior was observed at 250°C for holds longer than 1,000 s, and little to no strengthening was seen for shorter hold periods. At 250°C the failure strength was often less than the sliding frictional strength measured before the hold period (Figure 1h). This resulted in negative values of $\Delta\mu$.

The creep rate at the start of all hold periods was 0.1 μm/s which decayed rapidly so the average creep rate measured for 100 s holds at all temperatures clustered around 10^{-2} μm/s. The average creep rate decreased with hold duration but remains similar at all temperatures for holds ≤1,000 s. For holds longer than 1,000 s a clear increase in both the amount of creep and the associated average creep rate during the hold period is observed at 250°C (Figure 1h; Figure S4 in Supporting Information S1). For 500,000 s holds, the average creep rate at temperatures of 22–200°C clusters around 10^{-5} μm/s but is 10^{-4} μm/s at 250°C for the same hold duration.

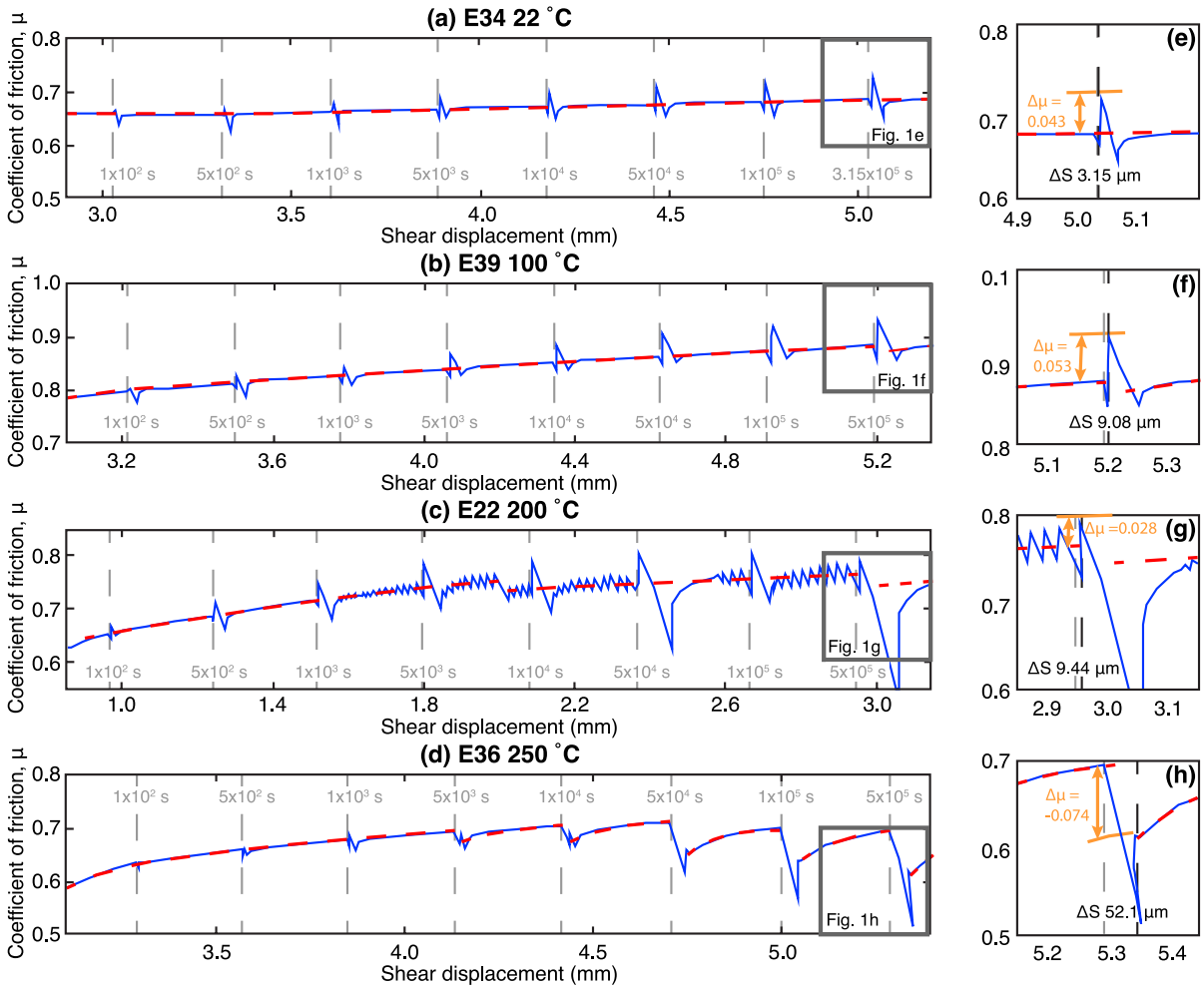

Figure 1. Evolution of coefficient of friction. Coefficient of friction (μ) versus displacement resolved on the fault surface for selected experiments on water-saturated samples run at temperatures of (a) 22°C, (b) 100°C, (c) 200°C, and (d) 250°C. Steady-state sliding secant friction is indicated by the red dashed lines. Hold periods are indicated by gray dashed lines with hold duration indicated. Dark gray boxes highlight the 500,000 s (315,000 s at 22°C) hold periods shown in e-h. The amount of creep that occurred during the hold period (ΔS) and change in friction ($\Delta\mu$) are shown. Full curves for all experiments examined in this study are provided in Figure S1 in Supporting Information S1.

3.2. Microstructural Observations

The sawcut surfaces of several samples that had undergone slide and hold periods were characterized using a scanning electron microscope (SEM) (Figure 3). Each of these specimens was removed from the pressure vessel at the end of an extended hold period (~100,000 s). For samples E34 (22°C) and E36 (250°C) the final hold period was preceded by a sequence of slides and holds reaching a cumulative displacement of 7 and 6.7 mm, respectively. E30 (200°C) had only experienced ~1 mm of shear displacement followed by a 109,000 s hold with no additional shearing.

In all three samples, abrasive wear features were apparent including slickenlines, grooved surfaces (Figures 3a and 3d), and gouge development (Figure 3b). At 200 and 250°C there was evidence of dissolution in the form of curved grain boundaries and possible pitting (Figures 3c and 3d). Additionally, at 250°C there was widespread evidence of secondary mineral precipitation (Figures 3e and 3f). Clusters of fibrous minerals were concentrated near the fluid borehole but were also seen in other areas. Secondary mineral development was not observed in the lower temperature experiments. Energy-dispersive X-ray measurements using the SEM indicated that some of the fibrous deposits contained Na, S, Ca, and Al (Figure 3e) while in other places they were enriched in Fe, Cr, Ni Cu, Zn, and Mg (Figure 3f).

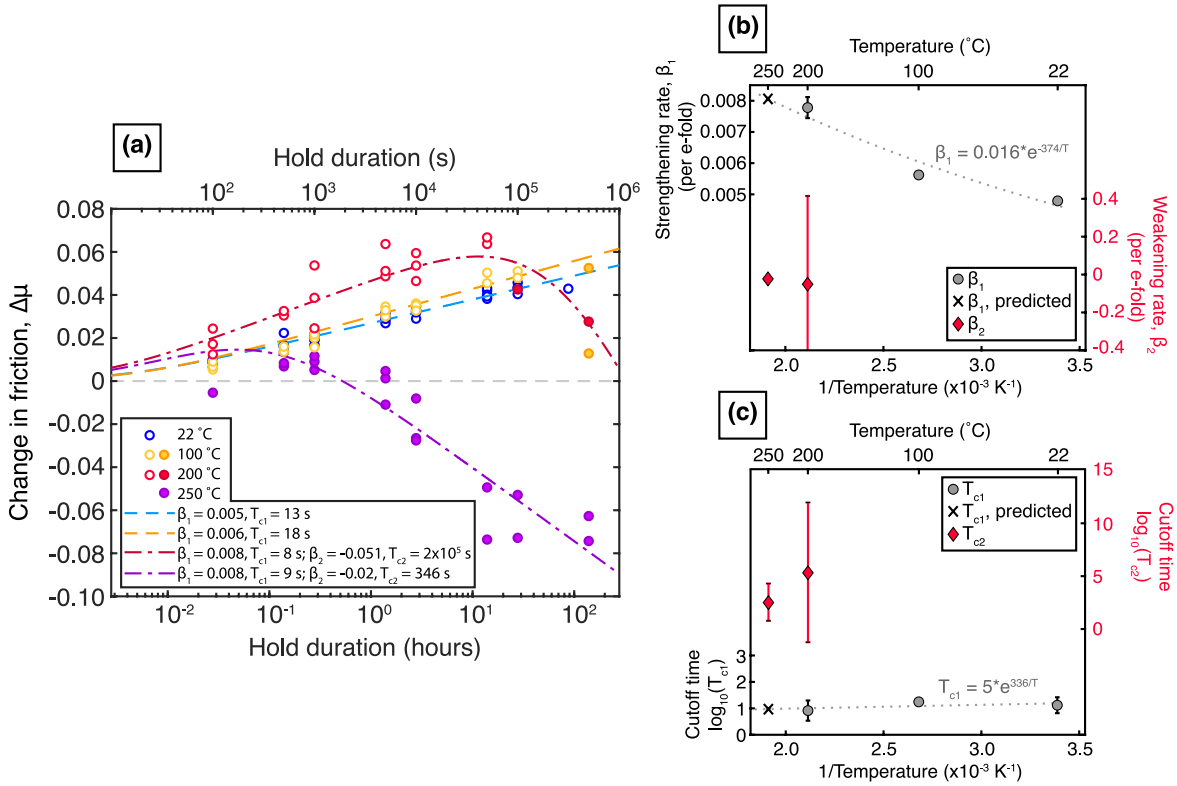

Figure 2. Time-dependent evolution of friction. (a) Changes in frictional strength ($\Delta\mu$), defined as the difference between failure strength and sliding friction preceding the hold period. Unfilled symbols indicate the data used to determine the initial restrengthening rates using Equation 1. Fits of Equations 1 and 2 are indicated by the dashed lines. The dependence of the resulting (b) healing (β_1) and weakening (β_2) rates and (c) cutoff times on temperature. The gray dashed line shows the fit of the Arrhenius type relation used to predict β_1 and Tc_1 at 250°C (indicated by x's). Error bars indicate 2σ standard error determined using jackknife resampling. If error bars are not visible, uncertainty is less than the marker size.

4. Discussion

4.1. Time-Dependent Friction

Previous studies have described SHS experiments on Westerly and other granitic samples. Most of these studies were conducted at room temperature and nominally dry conditions (Beeler et al., 1994; Dieterich, 1972; Ryan et al., 2018) with some work done on water-saturated samples (Carpenter et al., 2016). To the best of our knowledge SHS tests on granite at elevated temperatures (up to 600°C) have only been conducted in the presence of water vapor (Mitchell et al., 2013, 2016). These studies all reported time-dependent increases in $\Delta\mu$. An empirical expression can be used to quantify the rate of restrengthening:

$$\Delta\mu = \beta \ln\left(\frac{t_h}{t_c} + 1\right) \quad (1)$$

where β defines the time-dependent rate of restrengthening, t_h is the duration of the hold period, and t_c is the characteristic time delay beyond which the logarithmic dependence on time is observed (Dieterich, 1978; Nakatani & Scholz, 2004). At room temperature, healing rates for granitic rock determined from published data range from 0.003 per e-fold increase in hold time for a water-saturated, 2.6-mm-thick layer of Westerly granite gouge (Carpenter et al., 2016) to an average of 0.01 ± 0.001 per e-fold for initially bare-surface granite rock under nominally dry conditions (Beeler et al., 1994; Dieterich, 1972; Mitchell et al., 2013). In heated, nominally dry tests, β is 0.009 per e-fold at 100 and 200°C and 0.007 at 250°C (Mitchell et al., 2013). In all cases the cutoff time t_c is on the order of 1 s or less. Fitting Equation 1 to our experiments, using only data from hold periods where sliding friction was constant before and after the hold and $\Delta\mu$ increases with time, yields healing rates of 0.005, 0.006, and 0.008 per e-fold at 22, 100, and 200°C, respectively, with cutoff times on the order 1–10 s (Figure 2). This is generally consistent with previous work, suggesting the increase in strength with time occurs due to the growth

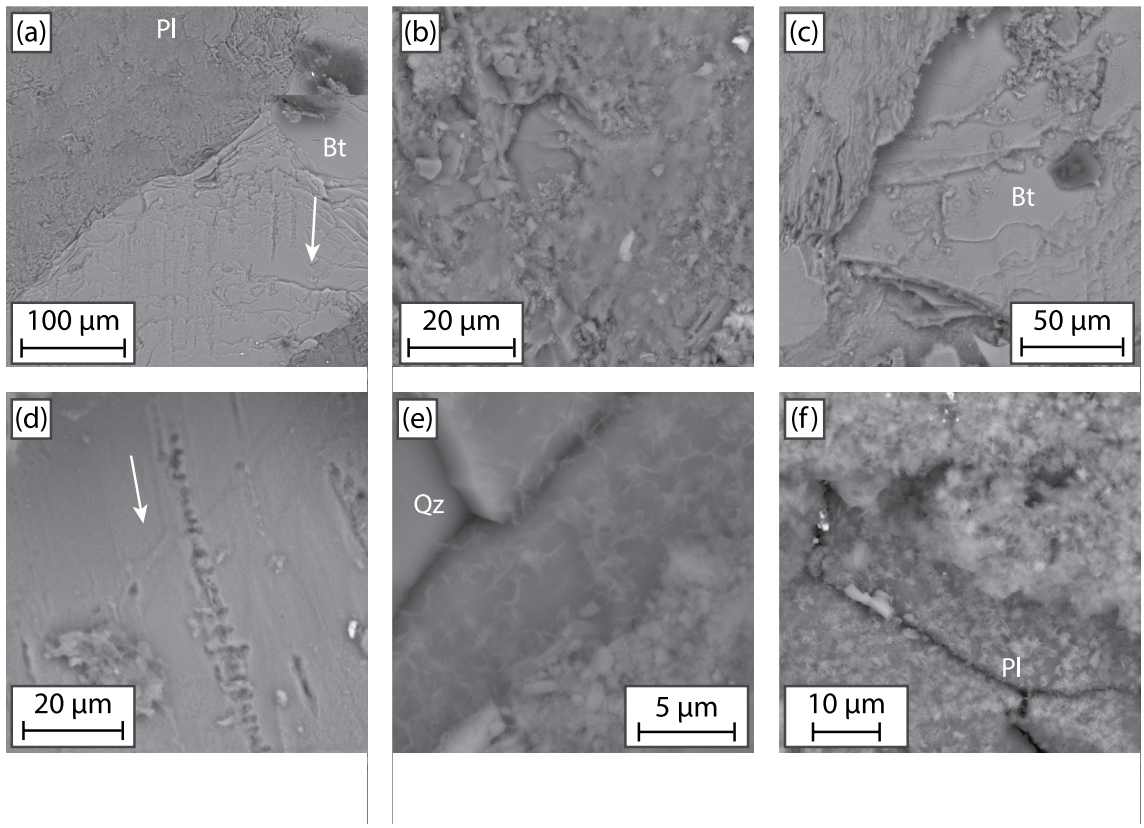

Figure 3. Backscattered electron images of the sawcut surfaces after an ~1 × 10^5 s hold period following shearing. (a) Slickenlines and grooves result from slip on the sawcut surface (E34, 22°C). White arrows show direction of slip. (b) A fine-grained gouge developed between the sawcut surfaces (E30, 200°C). (c) Rounded edges on cleavage planes in a biotite (Bt) crystal may result from dissolution (E36, 250°C). (d) Possible dissolution pits around a groove left by a dragging asperity (E36, 250°C). (e) Feathery growths of a secondary mineral enriched in Na, S, Ca, and Al on quartz (Qz) (E36, 250°C). (f) Abundant development of a secondary mineral deposit on a plagioclase (Pl) grain (E36, 250°C). The secondary mineral is enriched in Fe, Cr, Ni, Cu, Zn, and Mg.

of real contact area caused by mainly mechanical processes such as subcritical crack growth (e.g., Dieterich & Kilgore, 1994). We do not fit the short t_h data at 250°C since a period of initial restrengthening is not clearly observed.

A transition to time-dependent weakening has not previously been reported for granite at room temperature under either saturated or nominally dry conditions, or at elevated temperatures under nominally dry conditions. We conclude that the higher-temperature weakening behavior is caused by a different mechanism that is temperature-dependent and requires the presence of liquid-phase water. Hydrothermal SHS tests have been conducted on materials other than granite. In experiments on initially bare-surface quartz (Jeppson, Lockner, Beeler, & Hickman, 2023) and 3 mm thick layers of pure quartz gouge (>63 μm diameter) (Nakatani & Scholz, 2004) at temperatures up to 200°C only time-dependent increases in $\Delta\mu$ were observed. Olsen et al. (1998) conducted SHS tests on gouge layers composed of a mixture of quartz and labradorite sand at temperatures of 200 and 250°C (Olsen et al., 1998). While they did not observe time-dependent weakening they did not observe time-dependent strengthening either. This suggests that mineralogy is important to the underlying weakening mechanism.

Assuming the mechanisms controlling the observed strengthening and weakening are operating in parallel, Equation 1 can be expanded to capture the time-dependent evolution of friction observed in our data:

$$\Delta\mu = \beta_1 \ln\left(\frac{t_h}{t_{c1}} + 1\right) + \beta_2 \ln\left(\frac{t_h}{t_{c2}} + 1\right) \quad (2)$$

where β_1 and t_{c1} relate to the initial restrengthening behavior and β_2 and t_{c2} relate to the subsequent weakening behavior. Between 22 and 200°C we have sufficient data to constrain β_1 and t_{c1} but the process controlling β_2

and t_{c2} appears to be too sluggish to be constrained in the hold times available. At 250°C the weakening process dominates, masking any strengthening that occurs at short timescales. However, assuming that the strengthening mechanism is an Arrhenius process, as is expected, for example, for subcritical crack growth (Lawn, 1993), we extrapolate that β_1 and t_{c1} at 250°C are 0.008 and 9 s, respectively (Figures 2b and 2c). We note that Mitchell et al. (2013) identified a similar rate (0.007) for nominally dry Westerly granite at 250°C. This is consistent with a mechanism such as subcritical crack growth, that occurs in the presence of both liquid and gaseous water. Applying these constraints and fitting Equation 2 to the 250°C data yields $\beta_2 = -0.02$ per e-fold and $t_{c2} = 346$ s Equation 2 was also fit to the 200°C experiment, but due to the limited observations of weakening at this lower temperature β_2 and t_{c2} are poorly constrained. The data do indicate that the cutoff time of the weakening mechanism scales with temperature, consistent with an Arrhenius relation.

The significance of these rates and cutoff times is limited, as the parameters are interdependent, and none are well constrained. This empirical relation could be improved with additional measurements to define the underlying mechanisms and inclusion of expected rates for those mechanisms (e.g., Barbot, 2022). It is apparent that in polymineralic hydrothermal systems the evolution of frictional strength with time and temperature is complex because of the interactions among multiple mechanisms. Potentially competing mechanisms include pressure solution enhanced by the presence of phyllosilicates (e.g., Anzalone et al., 2006; Hickman & Evans, 1995; Meyer et al., 2006; Rutter & Wanten, 2000), chemical leaching, preferential dissolution of mechanically strong contacts, fabric development (Jordan, 1987), and secondary-mineral precipitation. We find clear evidence of secondary mineral phases developing at 250°C. Some mineral growths, like those shown in Figure 3f contain Cr, Fe, Ni, and Cu, suggesting they formed as a result of pore fluid reacting with the 17-4 steel end caps used in the sample assembly. These parts are located outside of the high temperature zone and should have limited effect on fault chemistry. Other secondary minerals lack these metals (e.g., Figure 3e). Weak secondary mineral phases could result in reduced friction (e.g., Bomberger, 2013; Carpenter et al., 2016; Morrow et al., 2017; Shreedharan et al., 2023), even at low concentrations, if they form preferentially at load-bearing contacts.

4.2. Rate and State Friction

In rate-stepping tests, Blanpied et al. (1995) observed a reduction in the frictional sliding strength of water-saturated samples at temperatures above 300°C. The temperature at which weakening is first observed increases with slip rate (their Figure 6). We observed that during 500,000 s hold periods at 250°C the average creep rate drops as low as 1×10^{-4} μm/s, significantly less than the slowest slip velocity (0.01 μm/s) examined by Blanpied et al. (1995). The same mechanisms that caused weakening in Blanpied et al.'s rate-stepping tests may also be responsible for weakening in our SHS experiments. Due to the very low creep rates attained during our extended hold periods, we are able to observe the weakening at temperatures as low as 200°C.

At temperatures above 350°C, rate-and-state (RS) modeling of Blanpied et al.'s (1995) rate-stepping tests required the addition of a second state variable (Blanpied et al., 1998). At 400°C, the scaling parameter for the first state variable, b_1, was positive and increased with temperature, whereas the parameter for the second state variable, b_2, was negative and became more negative with increasing temperature. While the rate constant (β) examined in this paper is not the same as the state variable scaling parameter (b), it is expected that $b \sim \beta$ (Ikari et al., 2016; Marone, 1998; Paterson & Wong, 2005), so a negative β implies that the corresponding b_2 would also be negative. Further, Blanpied et al. (1998) found that b_2 was associated with a large characteristic displacement (Dc) that was positively correlated with temperature, consistent with the prolonged evolution of sliding friction at 250°C in our SHS tests.

To further characterize the strength evolution in SHS tests we consider constraints on the RS friction parameters from the sequence of holds between 100 and 500,000 s at 250°C (Figure 1d). Strengthening during the hold is resolved only for holds greater than 500 s and less than 5,000 s (Figure 1d; Figure 2a). Figure 4a shows an RS simulation of a 1,000 s SHS hold using parameters comparable to those inferred by Blanpied et al. (1998) for rate stepping tests at 250°C ($a = 0.0125$, $b_1 = 0.005$, $Dc_1 = 0.25$ μm, $b_2 = 0.013$, $Dc_2 = 5$ μm). Blanpied et al. did not observe weakening at this temperature, requiring both b_1 and b_2 to be positive. The primary difference in parameter values used in simulations in Figure 4a lies in the values of Dc. Dc_1 is slightly outside of the uncertainty associated with the 1.6–8.6 μm range of Blanpied et al. (1998). The smaller Dc_1 is necessary to produce the post-peak slip event with stress drop following the 1,000 s hold (Figure 4a). Dc_2 is much smaller than the 560–908 μm range of Blanpied et al. (1998). Our data lack evidence for an equivalently long weakening distance following

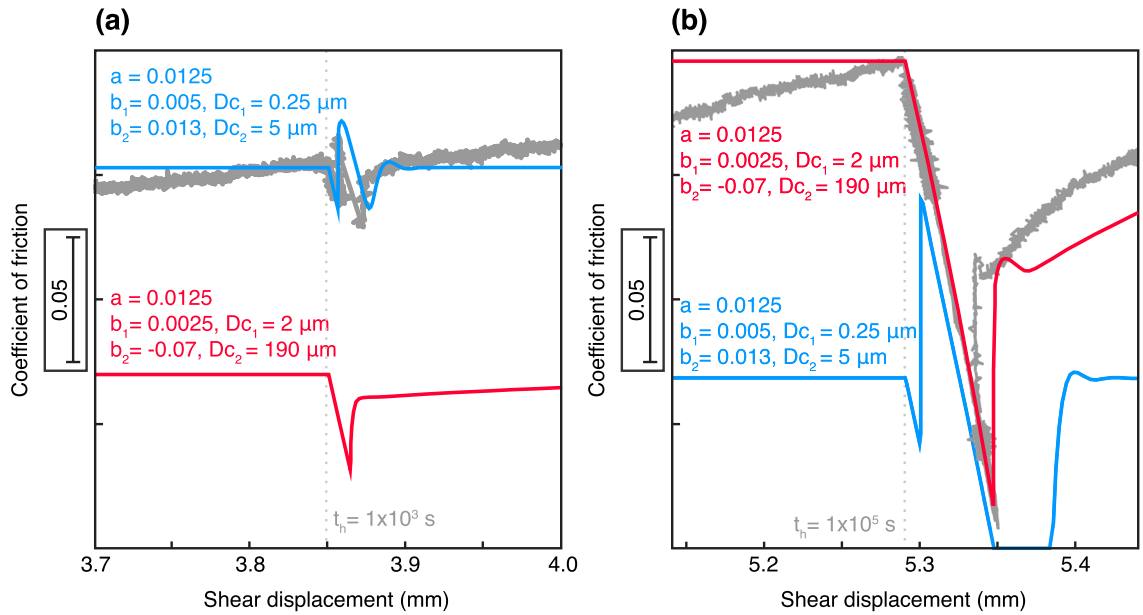

Figure 4. Slide-hold-slide simulations. RS slider block simulations of (a) 1,000 s and (b) 500,000 s holds at 250°C. Simulated loading velocity was 0.1 µm/s with a stiffness of 0.149 MPa/µm. Data from experiment E36 at 250°C are shown in dark gray. Simulations with RS parameters show blue curves using $a = 0.0125$, $b_1 = 0.005$, $Dc_1 = 0.25$ µm, $b_2 = 0.013$, $Dc_2 = 5$ µm and red curves using $a = 0.0125$, $b_1 = 0.0025$, $Dc_1 = 2$ µm, $b_2 = -0.07$, $D_{c2} = 190$ µm, respectively. Light-gray dashed line indicates the start of the hold period. In this case, blue model parameters fit the short hold data while red parameters provide better fit to the long hold data and indicate that time-stationary RS parameters are insufficient to represent the observations.

short hold periods. Otherwise, the parameters are within the published ranges. The data could also be reasonably well represented by an RS simulation with a single positive state variable. In contrast, for holds greater than 1,000 s the fault shows net strength losses over each SHS sequence by amounts that increase with hold duration (Figures 1d and 2a). These strength losses require significantly different RS parameters to adequately represent the weakening as shown in Figure 4b ($a = 0.0125$, $b_1 = 0.0025$, $Dc_1 = 2$ µm, $b_2 = -0.07$, $Dc_2 = 190$ µm). The largest change in parameters is a strongly negative b_2 with a long evolution distance Dc_2. The large negative b_2 is consistent with values inferred by Blanpied et al. (1998) at much higher temperatures (b_2 ranges from −0.03 to −0.14 at temperatures of 400–600°C). An extended description of the simulations is included in Supporting Information S1 (Text S3).

The parameters used to simulate the 1,000 s hold are comparable to those used for lower temperature experiments (Blanpied et al., 1998) whereas the parameters used for long hold times are dramatically different. This implies that significant hydrothermal alteration occurs in these 250°C experiments. The underlying mechanism appears to be a function of time, not slip, as is indicated by the dependence of the weakening behavior on hold duration and the change in creep rate after 1,000 s (Figure S4 in Supporting Information S1). Most formulations of the RS friction constitutive equations cannot accommodate time-dependent changes, as they lack a term that is representative of the t_c parameter present in Equation 2. Capturing the time-dependent weakening behavior would require reformulation of the RS friction equations to incorporate the characteristic time delay, possibly due to the strain-rate sensitivity of plastic yielding (e.g., Brechet & Estrin, 1994) or the reaction rate of a chemical process (e.g., Rimstidt & Barnes, 1980).

5. Conclusions

Frictional weakening is consistently observed at temperatures ≥200°C in hydrothermal SHS experiments and at temperatures ≥300°C in rate-stepping tests on Westerly granite (Blanpied et al., 1995). Rate and state friction simulations of long-duration holds at 250°C can only be represented using a two-state-variable RS friction model in which the second state variable is negative and associated with a large characteristic displacement (>100 µm). This negative state variable is not required to simulate shorter hold periods or lower temperatures, suggesting that significant hydrothermal alteration is occurring at 250°C. While the underlying mechanisms that control

the frictional behavior cannot be positively identified at this time, it is evident that the mechanisms must be water-assisted, temperature-dependent, and chemically complex with a characteristic time delay on the order of 1,000 s. This indicates that the observed frictional weakening is the product of a solution-transfer process. An understanding of the processes that control frictional behavior at hydrothermal conditions and how they relate to and can be incorporated in the RS friction equations will help us better understand and model earthquake behavior in a variety of materials and over a range of environmental conditions.

Data Availability Statement

The data presented in this paper can be found in Jeppson, Lockner, Beeler, and Moore (2023).

Acknowledgments
Funding was provided by the Department of Energy Office of Energy Efficiency & Renewable Energy to the University of Utah under Project DE-EE0007080 Enhanced Geothermal System Concept Testing and Development at the Milford City, Utah Frontier Observatory for Research in Geothermal Energy (Utah FORGE) site. Any use of trade, firm, or product names is for descriptive purposes only and does not imply endorsement by the U.S. Government.

References

Anzalone, A., Boles, J., Greene, G., Young, K., Israelachvili, J., & Alcantar, N. (2006). Confinged fluids and their role in pressure solution. *Chemical Geology*, *230*(3–4), 220–231. https://doi.org/10.1016/j.chemgeo.2006.02.027

Bakun, W. H., & Lindh, A. G. (1985). The Parkfield, California, earthquake prediction experiment. *Science*, *229*(4714), 619–624. https://doi.org/10.1126/science.229.4714.619

Barbot, S. (2022). A rate-state-and temperature-dependent friction law with competing healing mechanisms. *Journal of Geophysical Research: Solid Earth*, *127*(11), e2022JB025106. https://doi.org/10.1029/2022JB025106

Beeler, N. B., Tullis, T. E., & Weeks, J. D. (1994). The roles of time and displacement in the evolution effect in rock friction. *Geophysical Research Letters*, *21*(18), 1987–1990. https://doi.org/10.1029/94GL01599

Blanpied, M. L., Lockner, D. A., & Byerlee, J. D. (1991). Fault stability inferred from granite sliding experiments at hydrothermal conditions. *Geophysical Research Letters*, *18*(4), 609–612. https://doi.org/10.1029/91GL00469

Blanpied, M. L., Lockner, D. A., & Byerlee, J. D. (1995). Frictional slip of granite at hydrothermal conditions. *Journal of Geophysical Research*, *100*(B7), 13045–13064. https://doi.org/10.1029/95JB00862

Blanpied, M. L., Marone, C. J., Lockner, D. A., Byerlee, J. D., & King, D. P. (1998). Quantitative measure of the variation in fault rheology due to fluid-rock interactions. *Journal of Geophysical Research*, *103*(B5), 9691–9712. https://doi.org/10.1029/98jb00162

Bomberger, C. W. (2013). The influence of brines and temperature on the frictional properties of laboratory fault gouge. (Senior thesis). Pennsylvania State University. ScholarSphere Retrieved from https://scholarsphere.psu.edu/resources/3813f86c-f726-4385-8e17-113de60cf102

Brechet, Y., & Estrin, Y. (1994). The effect of strain rate sensitivitiy on dynamic friction of metals. *Scripta Metallurgica et Materialia*, *30*(11), 1449–1454. https://doi.org/10.1016/0956-716X(94)90244-5

Carpenter, B., Ikari, M., & Marone, C. (2016). Laboratory observations of time-dependent frictional strengthening and stress relaxation in natural and synthetic fault gouges. *Journal of Geophysical Research: Solid Earth*, *121*(2), 1183–1201. https://doi.org/10.1002/2015JB012136

Dieterich, J. H. (1972). Time-dependent friction in rocks. *Journal of Geophysical Research*, *77*(20), 3690–3697. https://doi.org/10.1029/jb077i020p03690

Dieterich, J. H. (1978). Time-dependent friction and the mechanics of stick-slip. *Pure and Applied Geophysics*, *116*(4–5), 790–806. https://doi.org/10.1007/bf00876539

Dieterich, J. H., & Kilgore, B. (1994). Direct observation of frictional contacts: New insights for state-dependent properties. *PAGEOPH*, *143*(1/2/3), 283–302. https://doi.org/10.1007/bf00874332

Hickman, S., & Evans, B. (1995). Kinetics of pressure solution at halite-silica interfaces and intergranular clay films. *Journal of Geophysical Research*, *100*(B7), 13113–13132. https://doi.org/10.1029/95jb00911

Ikari, M. J., Carpenter, B. M., & Marone, C. (2016). A microphysical interpretation of rate- and state-dependent friction for fault gouge. *Geochemistry, Geophysics, Geosystems*, *17*(5), 1660–1667. https://doi.org/10.1002/2016GC006286

Jeppson, T., Lockner, D., Beeler, N., & Hickman, S. (2023). Strength recovery in quartzite is controlled by changes in friction in experiments at hydrothermal conditions up to 200°C. *Journal of Geophysical Research: Solid Earth*, *128*(5), e2022JB025663. https://doi.org/10.1029/2022JB025663

Jeppson, T. N., Lockner, D. A., Beeler, N. M., & Moore, D. E. (2023). Slide-hold-slide experiments on Westerly granite at temperatures up to 250°C [Dataset]. U.S. Geological Survey Data Release. https://doi.org/10.5066/P9KNV1J8

Jordan, P. G. (1987). The deformational behaviour of bimineralic limestone—Halite aggregates. *Tectonophysics*, *135*(1–3), 185–197. https://doi.org/10.1016/0040-1951(87)90160-0

Karner, S. L., Marone, C., & Evans, B. (1997). Laboratory study of fault healing and lithification in simulated fault gouge under hydrothermal conditions. *Tectonophysics*, *277*(1–3), 41–55. https://doi.org/10.1016/S0040-1951(97)00077-2

Lawn, B. (1993). *Fracture of brittle solids. Cambridge solid state science series*. Cambridge University Press.

Marone, C. (1998). The effect of loading rate on static friction and the rate of fault healing during the earthquake cycle. *Nature*, *391*(6662), 69–72. https://doi.org/10.1038/34157

Meyer, E. E., Greene, G. W., Alcantar, N. A., Israelachvili, J. N., & Boles, J. R. (2006). Experimental investigation of the dissolution of quartz by a muscovite mica surface: Implications for pressure solution. *Journal of Geophysical Research*, *111*, B08202. https://doi.org/10.1029/2005JB004010

Mitchell, E. K., Fialko, Y., & Brown, K. M. (2013). Temperature dependence of frictional healing of Westerly granite: Experimental observations and numerical simulations. *Geochemistry, Geophysics, Geosystems*, *14*(3), 567–582. https://doi.org/10.1029/2012GC004241

Mitchell, E. K., Fialko, Y., & Brown, K. M. (2016). Velocity-weakening behavoir of Westerly granite at temperature up to 600°C. *Journal of Geophysical Research: Soild Earth*, *121*(9), 6932–6946. https://doi.org/10.1002/2016JB013081

Morrow, C. A., Moore, D. E., & Lockner, D. A. (2017). Frictional strength of wet and dry montmorillonite. *Journal of Geophysical Research: Solid Earth*, *122*(5), 3392–3409. https://doi.org/10.1002/2016JB013658

Nakatani, M., & Scholz, C. H. (2004). Frictional healing of quartz gouge under hydrothermal conditions: 1. Experimental evidence for solution transfer healing mechanisms. *Journal of Geophysical Research*, *109*, B07201. https://doi.org/10.1029/2001JB001522

Olsen, M. P., Scholz, C. H., & Léger, A. (1998). Healing and sealing of simulated fault gouge under hydrothermal conditions: Implications for fault healing. *Journal of Geophysical Research*, *103*(B4), 7421–7430. https://doi.org/10.1029/97JB03402

Paterson, M. S., & Wong, T. F. (2005). Friction and sliding phenomena. In *Experimental rock deformation—The Brittle field* (pp. 165–209). Springer -Verlag. https://doi.org/10.1007/b137431

Rimstidt, J. D., & Barnes, H. L. (1980). The kinetics of silica -water reactions. *Geochimica et Cosmochimia Atca*, *44*(11), 1683–1699. https://doi.org/10.1016/0016-7037(80)90220-3

Rutter, E. H., & Wanten, P. H. (2000). Experimental study of the compaction of phyllosilicate-bearing sand at elevated temperature and with controlled pore water pressure. *Journal of Sedimentary Research*, *70*(1), 107–116. https://doi.org/10.1306/2DC40902-0E47-11D7-8643000102C1865D

Ryan, K. L., Rivière, J., & Marone, C. (2018). The role of shear stress in fault healing and frictional aging. *Journal of Geophysical Research: Solid Earth*, *123*(12), 10479–10495. https://doi.org/10.1029/2018JB016296

Shreedharan, S., Saffer, D., Wallace, L. M., & Williams, C. (2023). Ultralow frictional healing explains recurring slow slip events. *Science*, *379*(6633), 712–717. https://doi.org/10.1126/science.adf4930

Tembe, S., Lockner, D. A., & Wong, T.-F. (2010). Effect of clay content and mineralogy on frictional sliding behavior of simulated gouges: Binary and ternary mixtures of quartz, illite, and montmorillonite. *Journal of Geophysical Research*, *115*, B03416. https://doi.org/10.1029/2009JB006383

Tenthorey, E., Cox, S. F., & Todd, H. F. (2003). Evolution of strength recovery and permeability during fluid-rock reaction in experimental fault zones. *Earth and Planetary Science Letters*, *206*(1–2), 161–172. https://doi.org/10.1016/S0012-821X(02)01082-8

Tesei, T., Collettini, C., Carpenter, B. M., Viti, C., & Marone, C. (2012). Frictional strength and healing behavior of phyllosilicate-rich faults. *Journal of Geophysical Research*, *117*(B9), B09402. https://doi.org/10.1029/2012JB009204

Uchida, N., & Bürgmann, R. (2019). Repeating earthquakes. *Annual Review of Earth and Planetary Sciences*, *47*(1), 305–332. https://doi.org/10.1146/annurev-earth-053018-060119

References From the Supporting Information

Beeler, N. M., & Lockner, D. A. (2003). Why earthquakes correlate weakly with Earth tides: The effects of periodic stress on the rate and probability of earthquake occurrence. *Journal of Geophysical Research*, *108*(B8), 2391. https://doi.org/10.1029/2001JB001518

Dieterich, J. H., & Linker, M. F. (1992). Fault stability under conditions of variable normal stress. *Geophysical Research Letters*, *19*(16), 1691–1694. https://doi.org/10.1029/92GL01821

Johnson, T., & Scholz, C. (1976). Dynamic properties of stick-slip friction of rock. *Journal of Geophysical Research*, *81*(5), 881–888. https://doi.org/10.1029/JB081i005p00881

Lockner, D. A., Kilgore, B. D., Beeler, N. M., & Moore, D. E. (2017). The transition from frictional sliding to shear melting in laboratory stick-slip experiments. In M. Y. Thomas, T. M. Mitchell, & H. S. Bhat (Eds.), *Fault zone dynamic processes*. https://doi.org/10.1002/9781119156895.ch6

Press, W. H., Flannery, B. P., Teukolsky, S. A., & Vetterling, W. T. (1986). *Numerical recipes: The art of scientific computing*. Cambridge University Press.

Rice, J. R., & Tse, S. T. (1986). Dynamic motion of a single degree of freedom system following a rate and state dependent friction law. *Journal of Geophysical Research*, *91*(B1), 521–530. https://doi.org/10.1029/JB091iB01p00521

Ruina, A. L. (1983). Slip instability and state variable friction laws. *Journal of Geophysical Research*, *88*(B12), 10359–10370. https://doi.org/10.1029/JB088iB12p10359

Walsh, J. B. (1971). Stiffness in faulting and in friction experiments. *Journal of Geophysical Research*, *76*(35), 8597–8598. https://doi.org/10.1029/JB076i035p08597